Iraqi Journal of Physics, 2025
https://doi.org/10.30723/ijp.v23i2.1304

Vol.23, No.3, PP.86-94
P-ISSN: 2070-4003
E-ISSN: 2664-5548

Flexible Near-Infrared Photodetector with High Sensitivity Using SnS Thin Film Deposited by Chemical Bath Method

Noor. M. Ibrahim[1,2*], Manal M. Abdullah[1] and Mohamed S. Mahdi[3]
[1]*Department of Physics, College of Science, University of Baghdad, Iraq*
[2]*Polymer Research Unit, Collage of Science, Mustansiriyah University, Baghdad, Iraq*
[3]*Research and Technology Center of Environment, Water, and Renewable Energy, Scientific Research Commission, Ministry of Higher Education and Scientific Research, Iraq*
[*]Corresponding author: noor_mohammed.i@uomustansiriyah.edu.iq

Abstract
The sensitivity of the photodetector is a crucial parameter when evaluating the performance of a cubic structure-based tin mono-sulfide (SnS) photodetector. However, achieving high sensitivity with a low-cost deposition technique for the SnS photodetector, which is based on a film grown on a flexible substrate, has been challenging. The primary aim of the present research is to fabricate a photodetector with higher sensitivity based on SnS thin film. The film was deposited onto a flexible polyester substrate utilizing a cheap and simple chemical bath deposition (CBD) method under 80 °C, pH 7.4, and 2.5 hours. The X-ray diffraction analysis showed that the film is made up of many small crystals and has a cubic shape, with an energy gap value of 1.56 eV. The photo-response properties were conducted upon illumination of near-infrared (NIR) 750 nm. The findings demonstrated that the photodetector has excellent stability and photo-response characteristics, involving a sensitivity of 1775, a rise time of 0.72 s, and a recovery time of 0.68 s. The fabricated flexible photodetector shows outstanding promise due to its excellent performance, cost-effectiveness, flexibility, and non-toxicity.

Article Info.

Keywords:
Flexible Substrate, Tin Mono Sulfide, Photosensitivity, Infrared, Photodetector.

Article history:
Received: Jun. 03, 2024
Revised: Dec. 04, 2024
Accepted:Dec. 21, 2024
Published:Sep. 01,2025

1. Introduction
Recently, there has been a substantial surge in scholarly interest in studying the optical and electrical properties of thin films composed of tin mono sulfide (SnS). The motive for this surge is due to its high absorption coefficient, around 10^4 cm^{-1} at the absorption fundamental edge, and high conductivity demonstrating a hole mobility of 90 $cm^2V^{-1}s^{-1}$ when utilized in electronic device fabrication [1, 2]. SnS is categorized under the chemical groups IV-VI, where Sn represents the cation, and S represents the anion. SnS is widely available, affordable, and non-toxic, making it a favored option for ecologically sustainable gadgets [3-7]. Moreover, it is of significant importance and is found in three distinct crystal forms: zinc blende, orthorhombic, and cubic [8-11].

Various methods can be employed to deposit films of SnS, including chemical bath deposition (CBD) [11-14], sputtering [15], dip deposition [16, 17], electrodeposition [18], vacuum evaporation [4, 19], spray pyrolysis [20], and chemical vapor deposition [21]. CBD is the preferred technique among researchers and practitioners because of its cost-effectiveness, ease of implementation, compatibility with extensive coating applications, and ability to operate at low temperatures, incurring little process expenses [13].

Previous studies have focused on the fabrication of SnS photodetectors based on growing films on rigid (glass) substrates [9, 22-31]. However, the sensitivity of these photodetectors was low. As a result, a novel approach is adopted in this study to fabricate a photodetector based on a grown SnS film on a flexible polyester substrate. The present flexible photodetector demonstrated high sensitivity level of 1775 and high stability under near-infrared illumination.

2. Experimental Part

2. 1. Films Preparation

The CBD method was utilized to deposit SnS film on a flexible polyester substrate. The deposition process involved using a solution of 0.15 M thioacetamide (C_2H_5NS) as a source for S^{-2} ions and 0.1 M of stannous chloride dehydrate ($SnCl_2.2H_2O$) as a source for Sn^{+2} ions. To prevent fast precipitate formation, 0.22 M of trisodium citrate dehydrate ($C_6H_5Na_3O_7.2H_2O$) was added as a complexing agent. An aqueous ammonium 25 % was added to the reaction solution to adjust its pH to 7.4. Before depositing the film, the polyester slide substrate was treated to ultrasonic cleaning using methanol, acetone, and deionized water for 30 minutes. The deposition process was performed at 80 °C for 2.5 hours. Subsequently, the film was rinsed using deionized water, followed by natural air-drying. Fig. 1 shows the flexible substrate and the deposited SnS film.

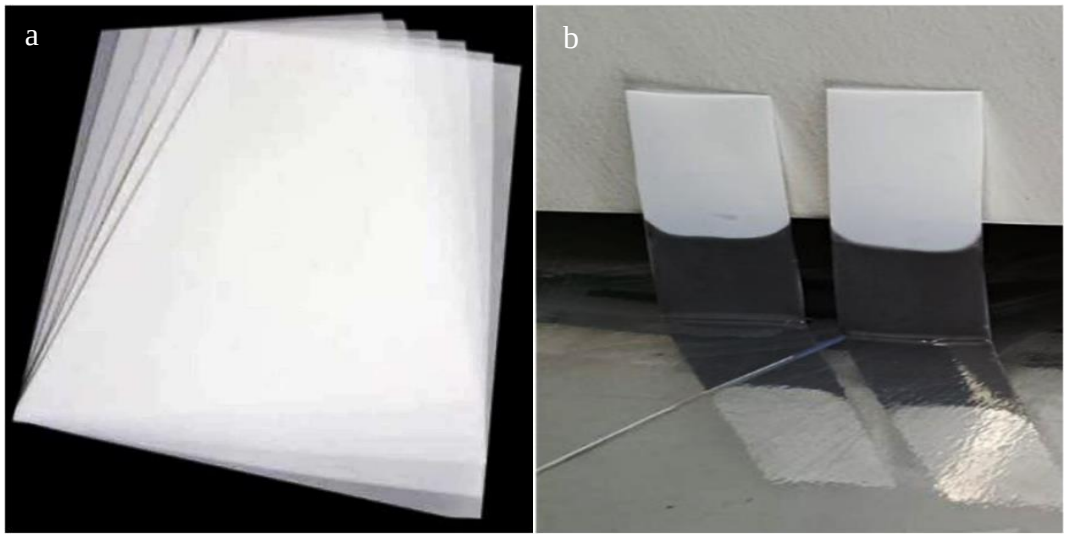

Figure 1: (a) An image illustrating the flexible substrates that are used as bases for thin-film deposition (b) An image of the deposited SnS thin-film.

2. 2. Film Characterization

The X-ray diffraction (XRD) patterns of the film and substrate were recorded using a diffractometer with CuKα radiation (λ = 1.5406 Å). Field emission scanning electron microscopy (FESEM) (f-50 FE-SEM) was used to study the film's surface shape. The films' thickness was measured with an Atomic Force Microscope (AFM) (a Nano Surf AG Core 2023). A spectrophotometer (Shimadzu-2601) was used to analyze the film's optical properties in the 350–1100 nm wavelength range. Furthermore, Keithley 2450 and light-emitting diode 750 nm were used to study the photo-response features of the photodetector.

3. Results and Discussion

3. 1. Crystal Structure

Fig. 2 (a, b) presents the X-ray diffraction patterns of the substrate and the deposited film. The peaks at 30.67°, 31.877°, and 32.68° are associated with the (400), (410), and (411) orientations of the π-SnS (SnS-CUB) structure, as indexed by PDF 86-9477 [28, 32-37]. Research conducted by Nair et al. [36] and Abutbul et al. [38, 39] has identified comparable peaks in the cubic phase. The XRD pattern of the film primarily displayed only these SnS peaks because other peaks may be obscured by a broad, intense peak of a polyester substrate from a 20° to 30° range.

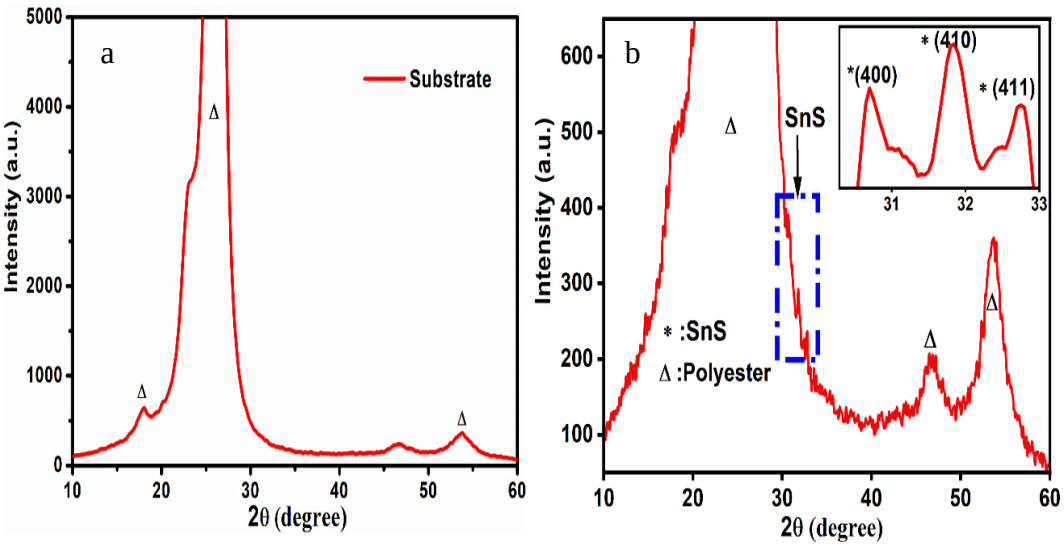

Figure 2: XRD patterns of polyester substrate and grown SnS film.

The crystallite size (D) of (410) and (411) planes were estimated using The Debye-Scherer equation [28]

$$D(\text{Å}) = \frac{K\lambda}{\beta \cos\theta} \quad (1)$$

where λ, θ and β denote wavelength, Bragg angle, and full width at half-maximum, respectively. The values of D were calculated to be 65 nm and 23 nm for the (410) and (411) orientations, respectively. These values align with previous findings [28]. To fabricate high-quality thin films for use in photodetector devices, it is necessary to reduce the dislocation density (δ) in the film, which can indicate the number of defects in the film. Micro-strain (ε) and dislocation density (δ) can be calculated using the following formulas [28].

$$\varepsilon = \frac{\beta}{4\tan\theta} \quad (2)$$

$$\delta = \frac{1}{D^2} \quad (3)$$

The number of crystallites per unit area (N) can be determined by using the equation [29]

$$N = \frac{t}{D^3} \quad (4)$$

where t is the thickness of the film. In a previous study, the atomic force microscopy (AFM) technique was employed to measure the thickness of film. This method involves creating a step-like structure by scratching the film with a sharp instrument. Since the film material is softer than the underlying substrate, it is assumed that the scratches completely remove the film in the affected areas, leaving behind distinct step edges. The height of these steps corresponds to the film's thickness. To ensure accuracy, multiple lateral AFM scans are conducted across the step structures, and an average film thickness is calculated [30]. In the present study, the thickness of the grown film was determined to be 371 nm.

The value of ε is equal to $\varepsilon = 1.95\times10^{-3}$, for δ =2.36×10^{12} lines.cm^{-2} and for N=1.35 $\times10^{14}$ cm^{-2} for orientation (410). The size of the crystallites is correlated with the presence of crystal defects. As the size of the crystallites increases, there is a decrease in dislocation, a reduction in crystal defects, and a decrease in boundaries. Consequently, this can enhance the electrical characteristics of the film [31]. The crystallite size of the film grown in this study exceeds the values reported in previous research studies [32].

3. 2. Surface Morphology

The FESEM image of the film is depicted in Fig. 3 (a). It can be seen that the film surface morphology contains dense grains that appear to cover the entire surface. Moreover, the grain distribution on the surface was homogenous and large. This morphology was seen in earlier studies for the cubic structure SnS film [23,33]. Additionally, the diameter of the grains ranged from 82 nm to 318 nm, as seen by the size distribution histogram in Fig. 3 (b).

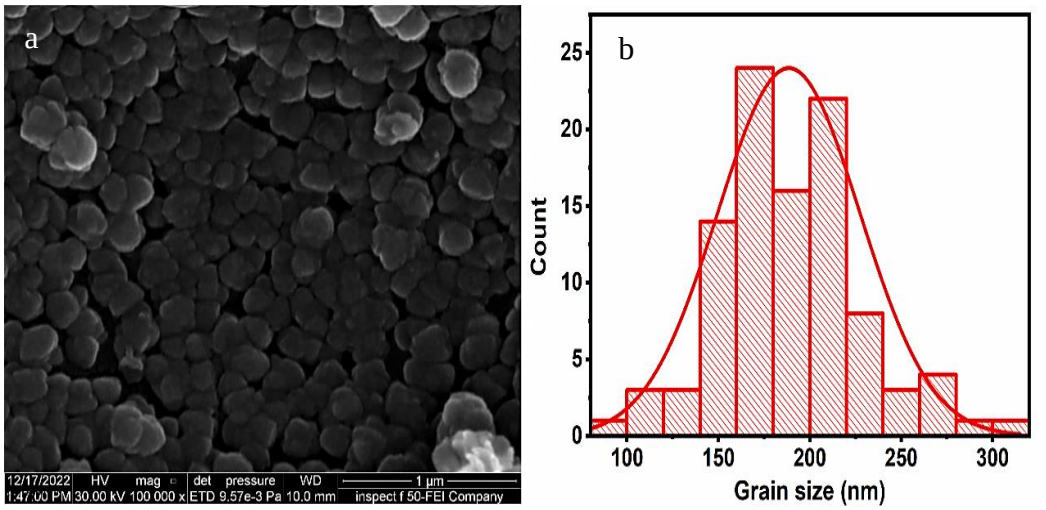

Figure 3: (a) FESEM image of prepared film SnS film, (b) Histogram distribution of grains diameter.

3. 3. Optical Properties

Fig. 4 (a) presents the optical transmittance spectrum of the SnS film on a polyester substrate, covering a wavelength range of 350-1100 nm. The transmittance value decreased with decreasing wavelength. Notably, the film demonstrated low transmittance in the near-infrared (NIR) spectral region. This characteristic makes the SnS film suitable for utilization in photodetector applications within this specific wavelength range. The transmittance (T) obtained from experimental measurements was used to determine the absorption coefficient (α) by the following equation [34]

$$\alpha = \frac{2.3026\log\left(\frac{1}{T}\right)}{t} \qquad (5)$$

In order to calculate the energy band gap from the transmission spectrum, the following relationship was used [19, 23]

$$\alpha h\nu = A\left(h\nu - E_g\right)^n \qquad (6)$$

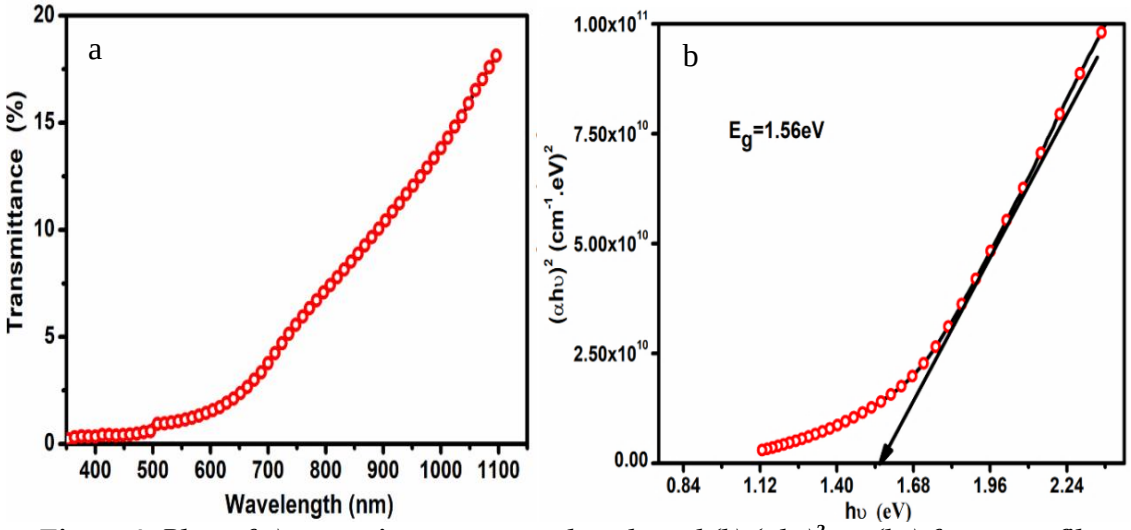

Figure 4: Plots of a) transmittance vs. wavelength, and (b) $(\alpha hv)^2$ vs. (hv) for grown film.

The absorption coefficient is denoted by α, the constant of Planck is represented by h, the frequency is symbolized by υ, the constant A is dependent on the transition probability, the energy bandgap is denoted by (E_g), and the parameter n varies based on the kind of transition. Fig. 4 (b) presents a graphical representation of the squared value of $(\alpha h\upsilon)^2$ plotted against hυ [18], based on the assumption that n equals (1/2). The direct energy bandgap can be determined by extrapolating the linear portion of the curve and identifying the intersection point with the (hυ) x-axis, yielding a value of 1.56 eV. The direct energy bandgap materials absorb light very efficiently, as photons can directly excite electrons from the valence band to the conduction band [23]. This property makes them suitable for solar cells and photodetectors, where efficient light absorption is crucial for generating electron-hole pairs.

3. 4. Photoresponse Measurements

The metal-semiconductor-metal (M-S-M) SnS photodetector was constructed with 120 nm-thick gold (Au) electrodes. Ion coating was used to deposit the electrodes on the film. Fig. 5 (a, b) shows the schematic of the device for studying the photoresponse and current-voltage (I-V) characteristics under both dark and light illumination 750 nm within the voltage range of -4 V to 4 V. The linear behavior of the (I-V) curve suggests that the Au electrodes establish ohmic contact with the SnS film because the work function of gold is about 5.1 eV [35], surpassing that of SnS, which ranges from 4.5 to 4.8 eV [36]. This difference facilitates efficient charge transfer and the establishment of an ohmic contact between the Au electrodes and the SnS thin film [37], which is crucial for the photodetector's performance. It is worth mentioning that the current value exhibits a substantial rise during near-infrared illumination compared to the dark state.

A photodetector application's repeatability and photoresponse speed are critical factors in defining its capacity. The photodetector stability was examined using 5 V bias voltage and 10 s ON/OFF switch cycle, as shown in Fig. 5 (c). The photodetector exhibits excellent repeatability and stability as its maximum current value remains constant and unvarying even after multiple cycles. The sudden drop in photocurrent during illumination can be attributed to spike noise at 10 and 20 seconds, which results from fluctuations in the light source's power during the switching process [38].

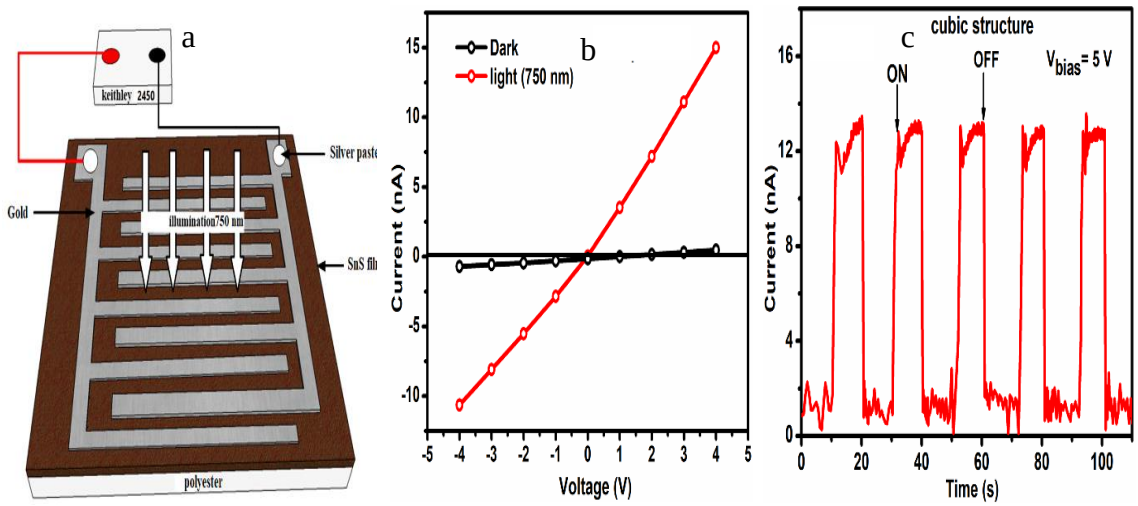

Figure 5: (a) the experimental setup for photoresponse measurements, (b, and c) the I-V and I-T characteristics of the photodetector in the dark and under illumination.

The ratio of an increase in current value under light to its value in darkness is referred to as a photodetector's sensitivity (S). The sensitivity can be expressed as follows [18, 20-22]

$$S = \frac{I_{ph}}{I_{dark}} x100 \qquad (7)$$

where $I_{ph} = I_{light} - I_{dark}$. I_{ph}, I_{dark} and I_{light} denote to photocurrent, dark, and under illumination current values, respectively. The S value was found to be 1775 for the photodetector. This value is highest when compared with previously fabricated SnS photodetectors glass (rigid) and PET (flexible) substrates [6, 17-23, 37, 39]. The photo-response time is crucial in assessing the photodetector's performance, and a substantially quicker response time has the capacity to expand the range of photodetector applications. The duration of a single on/off cycle was approximately 0.72 s for the rise time and 0.68 s for the decay time. The good photo-response characteristics of the present photodetector may be attributed to the large crystallite size (low dislocation density) of the photodetector film. The larger crystallite size for the deposited film on a polyester substrate leads to fewer grain boundaries and reduced defect density. These factors enhance charge carrier mobility and lifetime, contributing to the superior photoresponse characteristics of the present photodetector [40]. Table 1 compares the findings of the present photodetector to those of previously fabricated SnS photodetectors on glass (rigid) and PET (flexible) substrates.

Table 1: Comparative analysis of the findings of the present photodetector with previously manufactured SnS photodetectors on glass substrates.

Substrate	Crystal Structure	Crystallite size (D) (nm)	Bias Voltage (V)	Illumination Source	Power density (mW/cm^2)	Sensitivity %	Ref.
Glass	Orthorhombic	-	10	Tungsten halogen lamp	100	~250	[6]
Glass	Orthorhombic	33	5	Visible light	100	80	[17]
Glass	Orthorhombic	-	4	Tungsten halogen lamp	100	157	[18]
Glass	Orthorhombic	20.6	5	750 nm	38	260	[19]
Glass	Orthorhombic	34	5	532 nm	5	50	[20]
Glass	Orthorhombic	52	5	532 nm	–	~96	[21]
Glass	Orthorhombic	-	5	750 nm	38	170	[22]
Glass	Cubic	-	5	750 nm	38	700	[23]
PET	Orthorhombic	-	5	750 nm	38	404	[37]
PET	Orthorhombic		3	850 nm	55	304	[39]
Polyester	Cubic	65	5	750 nm	26	1775	This

4. Conclusions

The flexible photodetector is an important component in wearable devices due to its flexibility and lightness. This research aims to fabricate a low-cost, high-performance, flexible, near-infrared photodetector using a deposited SnS thin film on a polyester substrate. The film demonstrated excellent structural characteristics and high absorbance in the visible and near-infrared regions. These features enabled the photodetector to achieve a high sensitivity of 1775 under near-infrared illumination, as well as exceptional repeatability and stability. The research findings propose an effective approach to improve the performance of photodetectors and present a promising avenue for future advancements, such as flexible optoelectronic devices.

Acknowledgments

The authors would like to thank the University of Baghdad, College of Science, Department of Physics, for assisting us in this article.

Conflict of Interest

The authors declare that they have no conflict of interest.

References

1. C. Wu, K. Yao, Y. Guan, O. A. Ali, M. Cao, J. Huang, J. Lai, W. Shi, G. Hu, L. Wang, and Y. Shen, Mat. Sci. Semicond. Proce. **93**, 208 (2019). https://doi.org/10.1016/j.mssp.2019.01.008.
2. M. S. Mahdi, K. Ibrahim, A. Hmood, N. M. Ahmed, F. I. Mustafa, and S. A. Azzez, Mat. Lett. **200**, 10 (2017). https://doi.org/10.1016/j.matlet.2017.04.077.
3. G. S. Muhammed, M. M. Abdullah, and A. M. A. Al-Sammarraie Asian J. Chem. **30**, 1374 (2018). https://doi.org/10.14233/ajchem.2018.21262.
4. J. B. Johnson, H. Jones, B. S. Latham, J. D. Parker, R. D. Engelken, and C. Barber, Semicond. Sci. Technol. **14**, 501 (1999). https://doi.org/10.1088/0268-1242/14/6/303.
5. A. M. Kadim and W. R. Saleh, Iraqi J. Sci. **58**, 1207 (2017). https://ijs.uobaghdad.edu.iq/index.php/eijs/article/view/5844.
6. C. Gao, H. Shen, and L. Sun, Appl. Surf. Sci. **257**, 6750 (2011). https://doi.org/10.1016/j.apsusc.2011.02.116.
7. N. Koteeswara Reddy, M. Devika, and E. S. R. Gopal, Crit. Rev. Sol. Stat. Mat. Sci. **40**, 359 (2015). https://doi.org/10.1080/10408436.2015.1053601.

8. A. Tanusevski, Semicond. Sci. Technol. **18**, 501 (2003). https://doi.org/10.1088/0268-1242/18/6/318.
9. E. Guneri, C. Ulutas, F. Kirmizigul, G. Altindemir, F. Gode, and C. Gumus, Appl. Surf. Sci. **257**, 1189 (2010). https://doi.org/10.1016/j.apsusc.2010.07.104.
10. E. Turan, M. Kul, A. S. Aybek, and M. Zor, J. Phys. D Appl. Phys. **42**, 245408 (2009). https://doi.org/10.1088/0022-3727/42/24/245408.
11. B. A. Tedla, Neuro Quantology **20**, 6111 (2022). https://doi.org/10.14704/nq.2022.20.6. NQ22616.
12. A. F. Rauuf and K. A. Aadim, Iraqi J. Sci. **64**, 2877 (2023). https://doi.org/10.24996/ijs.2023.64.6.18.
13. W. R. Saleh, S. M. Hassan, S. Y. Al-Dabagh, and M. A. Marwa, Nano Hybr. Compos. **33**, 93 (2021). https://doi.org/10.4028/www.scientific.net/NHC.33.93.
14. M. Ichimura, K. Takeuchi, Y. Ono, and E. Arai, Thin Sol. Fil. **361-362**, 98 (2000). https://doi.org/10.1016/S0040-6090(99)00798-1.
15. 15. M. Calixto-Rodriguez, H. Martinez, A. Sanchez-Juarez, J. Campos-Alvarez, A. Tiburcio-Silver, and M. E. Calixto, Thin Sol. Fil. **517**, 2497 (2009). https://doi.org/10.1016/j.tsf.2008.11.026.
16. A. Ortiz, J. C. Alonso, M. Garcia, and J. Toriz, Semicond. Sci. Technol. **11**, 243 (1996). https://doi.org/10.1088/0268-1242/11/2/017.
17. T. S. Reddy and M. C. S. Kumar, RSC Adv. **6**, 95680 (2016). https://doi.org/10.1039/C6RA20129F.
18. M. Cao, C. Wu, K. Yao, J. Jing, J. Huang, M. Cao, J. Zhang, J. Lai, O. Ali, L. Wang, and Y. Shen, Mat. Res. Bullet. **104**, 244 (2018). https://doi.org/10.1016/j.materresbull.2018.03.039.
19. M. S. Mahdi, A. Hmood, K. Ibrahim, N. M. Ahmed, and M. Bououdina, Superlatt. Microstruct. **128**, 170 (2019). https://doi.org/10.1016/j.spmi.2019.01.031.
20. D. Alagarasan, S. S. Hegde, S. Varadharajaperumal, R. Aadhavan, R. Naik, M. Shkir, H. Algarni, and R. Ganesan, Phys. Scr. **97**, 065814 (2022). https://doi.org/10.1088/1402-4896/ac6d19.
21. R. Balakarthikeyan, A. Santhanam, A. Khan, A. M. El-Toni, A. A. Ansari, A. Imran, M. Shkir, and S. Alfaify, Optik **244**, 167460 (2021). https://doi.org/10.1016/j.ijleo.2021.167460.
22. M. S. Mahdi, K. Ibrahim, N. M. Ahmed, A. Hmood, and S. A. Azzez, Sol. Stat. Phenom. **290**, 220 (2019). https://doi.org/10.4028/www.scientific.net/ssp.290.220.
23. M. S. Mahdi, K. Ibrahim, N. M. Ahmed, A. Hmood, S. A. Azzez, F. I. Mustafa, and M. Bououdina, Mat. Lett. **210**, 279 (2018). https://doi.org/10.1016/j.matlet.2017.09.049.
24. Khan, N., Javed, A., Bashir, M., & Bashir, S., Results in Optics. **14, 100610** (2024). https://doi.org/10.1016/j.rio.2024.100610.
25. Harshal V Barkale, Aditya Narayn, Gowtham Polumati, Parikshit Sahatiya, Nilanjan Dey, ACS Applied Electronic Materials, **7,** 6440 (2024). https://doi.org/10.1021/acsaelm.5c00710.
26. R. E. Abutbul, A. R. Garcia-Angelmo, Z. Burshtein, M. T. S. Nair, P. K. Nair, and Y. Golan, CrystEngComm **18**, 5188 (2016). https://doi.org/10.1039/C6CE00647G.
27. R. E. Abutbul, E. Segev, L. Zeiri, V. Ezersky, G. Makov, and Y. Golan, RSC Adv. **6**, 5848 (2016). https://doi.org/10.1039/C5RA23092F.
28. P. M. B. Devi, G. P. Reddy, and K. T. R. Reddy, J. Semicond. **40**, 052101 (2019). https://doi.org/10.1088/1674-4926/40/5/052101.
29. M. M. El-Nahass, Z. El-Gohary, and H. S. Soliman, Opt. Laser Tech. **35**, 523 (2003). https://doi.org/10.1016/S0030-3992(03)00068-9.
30. F. Gode, E. Guneri, and O. Baglayan, Appl. Surf. Sci. **318**, 227 (2014). https://doi.org/10.1016/j.apsusc.2014.04.128.
31. A. R. Garcia-Angelmo, R. Romano-Trujillo, J. Campos-Álvarez, O. Gomez-Daza, M. T. S. Nair, and P. K. Nair, Phys. Stat. Sol. A **212**, 2332 (2015). https://doi.org/10.1002/pssa.201532405.
32. S. John, M. Francis, R. M. Ap, and V. Geetha, Indian J. Pure Appl. Phys. **61**, 326 (2023). https://doi.org/10.56042/ijpap.v61i5.70933.
33. D. Li, L. Dai, X. Ren, F. Ji, Q. Sun, Y. Zhang, and L. Ci, Energy Environ. Sci.,**14, 424** (2021). https://doi.org/10.1039/D0EE02919J.
34. S. Suresh, J. Cryst. Proces. Tech. **3**, 5 (2013). https://doi.org/10.4236/jcpt.2013.33014.
35. B. Aghili, S. Rahbarpour, M. Berahman, and A. Horri, J. Phys. Chem. C **128**, 8077 (2024). https://doi.org/10.1021/acs.jpcc.4c01068.
36. M. S. Nithyapriya, S. Athithya, S. M. Mariappan, S. Harish, M. Navaneethan, and J. Archana, Emergent. Mat. **7**, 867 (2024). https://doi.org/10.1007/s42247-023-00618-5.
37. Jadhav, C. D., Patil, G. P., Amar, M., Lyssenko, S., & Minnes, R., Journal of Power. **623**, 235496 (2024). https://doi.org/10.1016/j.jpowsour.2024.235496.
38. A. Parbatani, E. S. Song, F. Yang, and B. Yu, Nanoscale **10**, 15003 (2018). https://doi.org/10.1039/C8NR04047H.
39. M. S. Mahdi, K. H. Latif, A. A. Jabor, K. Ibrahim, N. M. Ahmed, A. Hmood, F. I. Mustafa, and M. Bououdina, J. Elect. Mat. **49**, 5824 (2020). https://doi.org/10.1007/s11664-020-08367-5.

40. K. M. Gupta and N. Gupta, *Advanced Semiconducting Materials and Devices* (Cham, Springer, 2016).

كاشف ضوئي مرن للأشعة تحت الحمراء القريبة ذو حساسية عالية باستخدام غشاء رقيق من أحادي كبريتيد القصدير مرسب بطريقة الحمام الكيميائي

نور محمد إبراهيم[1،2] ومنال مدحت عبد الله[1] ومحمد صالح مهدي[3]

[1،2]قسم الفيزياء، كلية العلوم، جامعة بغداد، العراق

[2]وحدة بحوث البوليمرات، كلية العلوم، الجامعة المستنصرية، بغداد، العراق

[3]مركز بحوث وتكنولوجيا البيئة والماء والطاقة المتجددة، هيئة البحث العلمي، وزارة التعليم العالي والبحث العلمي، العراق

الخلاصة

تعد حساسية الكاشف الضوئي معلمة حاسمة عند تقييم أداء الكاشف الضوئي أحادي كبريتيد القصدير القائم على البنية المكعبة. ومع ذلك، فإن تحقيق حساسية عالية القيمة باستخدام تقنية ترسيب منخفضة التكلفة للكاشف الضوئي أحادي كبريتيد القصدير استنادًا إلى الفيلم المزروع على ركيزة مرنة كان أمرًا صعبًا. الهدف الأساسي من هذا البحث هو تصنيع كاشف ضوئي أحادي كبريتيد القصدير ذو حساسية أعلى من خلال استخدام غشاء رقيق أحادي كبريتيد القصدير مزروع على ركيزة بوليستر مرنة. تم ترسيب الفيلم باستخدام تقنية الترسيب بالحمام الكيميائي (CBD) تحت ظروف 80 درجة مئوية، ودرجة الحموضة 7.4، و2.5 ساعة. أكد تحليل حيود الأشعة السينية طبيعة الفيلم متعددة البلورات وتركيبه البلوري المكعب، مع وجود فجوة طاقة تبلغ 1.56 فولت. تم قياس خصائص الاستجابة الضوئية وتحليلها باستخدام إضاءة الأشعة تحت الحمراء القريبة (NIR) (750 نانومتر). أظهر الكاشف الضوئي المقدم ثباتًا ممتازًا وخصائص الاستجابة الضوئية، بما في ذلك الحساسية (1775)، ووقت الارتفاع (0.72 ثانية)، ووقت الاضمحلال (0.68 ثانية) عند 5 فولت من جهد التحيز. يعد الكاشف الضوئي المرن المُصنَّع واعدًا جدًا استنادًا إلى أدائه الجيد ومرونته وتكلفته المنخفضة وطبيعته غير السامة.

الكلمات المفتاحية: الركيزة المرنة، أحادي كبريتيد القصدير، حساسية للضوء، الأشعة تحت الحمراء، الكاشف.